
Model-Based Control with Sparse Neural Dynamics

Ziang Liu^{1,2} Genggeng Zhou^{2*} Jeff He^{2*} Tobia Marcucci³

Li Fei-Fei² Jiajun Wu² Yunzhu Li^{2,4}

¹Cornell University ²Stanford University

³Massachusetts Institute of Technology

⁴University of Illinois Urbana-Champaign

ziangliu@cs.cornell.edu

{g9zhou, jeff2024}@stanford.edu

tobiam@mit.edu

{feifeili, jiajunwu}@cs.stanford.edu

yunzhuli@illinois.edu

Abstract

Learning predictive models from observations using deep neural networks (DNNs) is a promising new approach to many real-world planning and control problems. However, common DNNs are too unstructured for effective planning, and current control methods typically rely on extensive sampling or local gradient descent. In this paper, we propose a new framework for integrated model learning and predictive control that is amenable to efficient optimization algorithms. Specifically, we start with a ReLU neural model of the system dynamics and, with minimal losses in prediction accuracy, we gradually sparsify it by removing redundant neurons. This discrete sparsification process is approximated as a continuous problem, enabling an end-to-end optimization of both the model architecture and the weight parameters. The sparsified model is subsequently used by a mixed-integer predictive controller, which represents the neuron activations as binary variables and employs efficient branch-and-bound algorithms. Our framework is applicable to a wide variety of DNNs, from simple multilayer perceptrons to complex graph neural dynamics. It can efficiently handle tasks involving complicated contact dynamics, such as object pushing, compositional object sorting, and manipulation of deformable objects. Numerical and hardware experiments show that, despite the aggressive sparsification, our framework can deliver better closed-loop performance than existing state-of-the-art methods. [†]

1 Introduction

Our mental model of the physical environment enables us to easily carry out a broad spectrum of complex control tasks, many of which lie far beyond the capabilities of present-day robots [35]. It is, therefore, desirable to build predictive models of the environment from observations and develop optimization algorithms to help the robots understand the impact of their actions and make effective plans to achieve a given goal. Physics-based models [27, 79] have excellent generalization ability but typically require full-state information of the environment, which is hard and sometimes impossible to obtain in complicated robotic (manipulation) tasks. Learning-based dynamics modeling circumvents the problem by learning a predictive model directly from raw sensory observations, and recent successes are rooted in the use of deep neural networks (DNNs) as the functional class [15, 22, 60, 51]. Despite their improved prediction accuracy, DNNs are highly nonlinear,

*denotes equal contribution

[†]Please see our website at robopil.github.io/Sparse-Dynamics/ for additional visualizations.

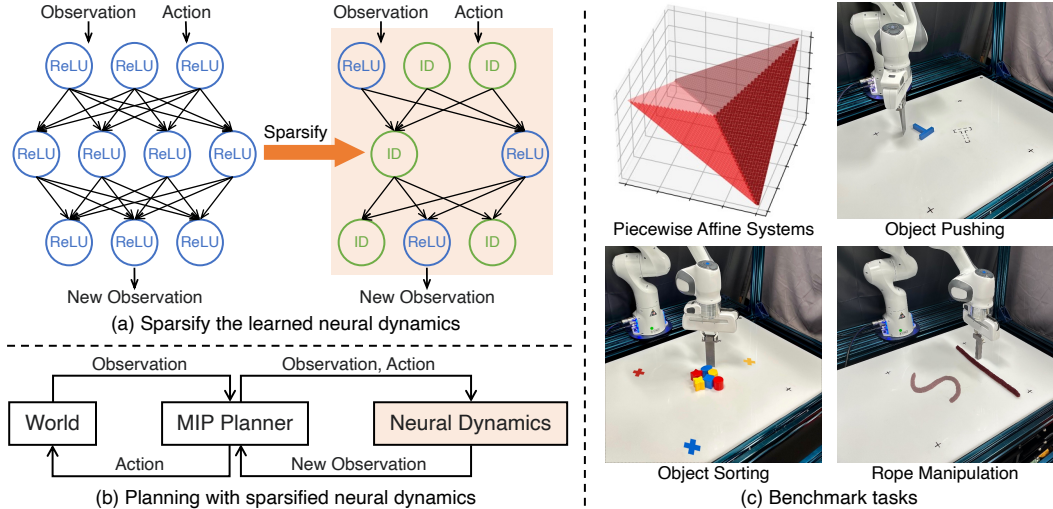


Figure 1: **Model-based control with sparse neural dynamics.** (a) Our framework sparsifies the neural dynamics models by either removing neurons or replacing ReLU activation functions with identity mappings (ID). (b) The sparsified models enable the use of efficient MIP methods for planning, which can achieve better closed-loop performance than sampling-based alternatives commonly used in model-based RL. (c) We evaluate our framework on various dynamical systems that involve complex contact dynamics, including tasks like object pushing and sorting, and manipulating a deformable rope.

making model-based planning with neural dynamics models very challenging. Existing methods often rely on extensive sampling or local gradient descent to compute control signals, and can be ineffective for complicated and long-horizon planning tasks.

Compared to DNNs, simpler models like linear models are amenable to optimization tools with better guarantees, but often struggle to accurately fit observation data. An important question arises: how precise do these models need to be when employed within a feedback control loop? The cognitive science community offers substantial evidence suggesting that humans do not maintain highly accurate mental models; nevertheless, these less precise models can be effectively used with environmental feedback [31, 11]. This notion is also key in control-oriented system identification [26, 48] and model order reduction [59, 66]. The framework from Li et al. [41] trades model expressiveness and precision for more efficient and effective optimization-based planning through the learning of compositional Koopman operators. However, their approach is limited by the linearity of the representation in the Koopman embedding space and struggles with more complex dynamics.

In this paper, we propose a framework for integrated model learning and control that trades off prediction accuracy for the use of principled optimization tools. Drawing inspiration from the neural network pruning and neural architecture search communities [23, 58, 17, 6, 44], we start from a neural network with ReLU activation functions and gradually reduce the nonlinearity of the model by removing ReLU units or replacing them with identity mappings (Figure 1a). This yields a highly sparsified neural dynamics model, that is amenable to model-based control using state-of-the-art solvers for mixed-integer programming (MIP) (Figure 1b).

We present examples where the proposed sparsification pipeline can determine region partition and uncover the underlying system for simple piecewise affine systems. Moreover, it can maintain high prediction accuracy for more complex manipulation tasks, using a considerably smaller portion of the original nonlinearities. Importantly, our approach allows the joint optimization of the network architecture and weight parameters. This yields a spectrum of models with varying degrees of sparsification. Within this spectrum, we can identify the simplest model that is adequate to meet the requirements of the downstream closed-loop control task.

Our contributions can be summarized as follows: (i) We propose a novel formulation for identifying the dynamics model from observation data. For this step, we introduce a continuous approximation of the sparsification problem, enabling end-to-end gradient-based optimization for both the model class and the model parameters (Figure 1a). (ii) By having significantly fewer ReLU units than

the full model, the sparsified dynamics model allows us to solve the predictive-control problems using efficient MIP solvers (Figure 1b). This can lead to better closed-loop performance compared to both model-free and model-based reinforcement learning (RL) baselines. (iii) Our framework can be applied to many types of neural dynamics, from vanilla multilayer perceptrons (MLPs) to complex graph neural networks (GNNs). We show its effectiveness in a variety of simulated and real-world manipulation tasks with complex contact dynamics, such as object pushing and sorting, and manipulation of deformable objects (Figure 1c).

2 Related Work

Model learning for planning and control. Model-based RL agents learn predictive models of their environment from observations, which are subsequently used to plan their actions [10, 57]. Recent successes in this domain often heavily rely on DNNs, exhibiting remarkable planning and control results in challenging simulated tasks [63], as well as complex real-world locomotion and manipulation tasks [37, 60]. Many of these studies draw inspiration from advancements in computer vision, learning dynamics models directly in pixel-space [16, 12, 13, 77, 67], keypoint representation [34, 51, 42], particle/mesh representation [39, 65, 28], or low-dimensional latent space [70, 1, 22, 21, 63, 75]. While previous works typically assume that the model class is given and fixed during the optimization process, our work puts emphasis on finding the desired model class via an aggressive network sparsification, to support optimization tools with better guarantees. We are willing to sacrifice the prediction accuracy for better closed-loop performance using more principled optimization techniques.

Network sparsification. The concept of neural network sparsification is not new and traces back to the 1990s [36]. Since then, extensive research has been conducted, falling broadly into two categories: network pruning [24, 23, 72, 58, 38, 25, 3, 47, 17, 46, 6, 78] and neural architecture search [80, 9, 43, 14, 69]. Many of these studies have demonstrated that fitting an overparameterized model before pruning yields better results than directly fitting a smaller model. Our formulation is closely related to DARTS [44] and FBNet [74], which both seek a continuous approximation of the discrete search process. However, unlike typical structured network compression methods, which try to remove as many units as possible, our goal here is to minimize the model nonlinearity. To this end, our method also permits the substitution of ReLU activations with identity mappings. This leaves the number of units unchanged but makes the downstream optimization problem much simpler.

Mixed-integer modeling of neural networks. The input-output map of a neural network with ReLU activations is a piecewise affine function that can be modeled exactly through a set of mixed-integer linear inequalities. This allows us to use highly-effective MIP solvers for the solution of the model-based control problem. The same observation has been leveraged before for robustness analysis of DNNs [68, 76] and for providing safety guarantees for control with neural dynamics models [71], while the efficiency of these mixed-integer models has been thoroughly studied in [2].

3 Method

In this section, we describe our methods for learning a dynamics model using environmental observations and for sparsifying DNNs through a continuous approximation of the discrete pruning process. Then we discuss how the sparsified model can be used by an MIP solver for trajectory optimization and closed-loop control.

3.1 Learning a dynamics model over the observation space

Assume we have a dataset $\mathcal{D} = \{(y_t^m, u_t^m) \mid t = 1, \dots, T, m = 1, \dots, M\}$ collected via interactions with the environment, where y_t^m and u_t^m denote the observation and action obtained at time t in trajectory m . Our goal is to learn an autoregressive model \hat{f}_θ , parameterized by θ , as a proxy of the real dynamics that takes a small sequence of observations and actions from time t' to the current time t , and predicts the next observation at time $t + 1$:

$$\hat{y}_{t+1}^m = \hat{f}_\theta(y_{t':t}^m, u_{t':t}^m). \tag{1}$$

We optimize the parameter θ to minimize the simulation error that describes the long-term discrepancy between the prediction and the actual observation:

$$\mathcal{L}(\theta) = \sum_{m=1}^M \sum_t \|y_{t+1}^m - \hat{f}_\theta(\hat{y}_{t':t}^m, u_{t':t}^m)\|_2^2. \quad (2)$$

3.2 Neural network sparsification by removing or replacing ReLU activations

We instantiate the transition function \hat{f}_θ as a ReLU neural network with N hidden layers. Let us denote the number of neurons in the i^{th} layer as N_i . When given an input $x = (y_{t':t}^m, u_{t':t}^m)$, we denote the value of the j^{th} neuron in layer i before the ReLU activation as x_{ij} . Regular ReLU neural networks apply the rectifier function to every x_{ij} and obtain the activation value using $x_{ij}^+ = h_{ij}(x_{ij}) \equiv \text{ReLU}(x_{ij}) \triangleq \max(0, x_{ij})$. The nonlinearity introduced by the ReLU function allows the neural networks to fit the dataset but makes the downstream planning and control tasks more challenging. As suggested by many prior works in the field of neural network compression [23, 17], a lot of these ReLUs are redundant and can be removed with minimal effects on the prediction accuracy. In this work, we reduce the number of ReLU functions by replacing the function h_{ij} with either an identity mapping $\text{ID}(x_{ij}) \triangleq x_{ij}$ or a zero function $\text{Zero}(x_{ij}) \triangleq 0$, where the latter is equivalent to removing the neuron (Figure 1a).

We divide the parameters in \hat{f}_θ into two vectors, $\theta = (\omega, \alpha)$. The vector ω collects the weight matrices and the bias terms. The vector α consists of a set of integer variables that parameterize the architecture of the neural network: $\alpha = \{\alpha_{ij} \in \{1, 2, 3\} \mid i = 1, \dots, N, j = 1, \dots, N_i\}$, such that

$$h_{ij}(x_{ij}) = \begin{cases} \text{ReLU}(x_{ij}) & \text{if } \alpha_{ij} = 1 \\ \text{ID}(x_{ij}) & \text{if } \alpha_{ij} = 2 \\ \text{Zero}(x_{ij}) & \text{if } \alpha_{ij} = 3 \end{cases}. \quad (3)$$

The sparsification problem can then be formulated as the following MIP:

$$\min_{\theta=(\omega, \alpha)} \mathcal{L}(\theta) \quad \text{s.t.} \quad \sum_{i=1}^N \sum_{j=1}^{N_i} \mathbb{1}(\alpha_{ij} = 1) \leq \varepsilon, \quad (4)$$

where $\mathbb{1}$ is the indicator function, and the value of ε decides the number of regular ReLU functions that are allowed to remain in the neural network.

3.3 Reparameterizing the categorical distribution using Gumbel-Softmax

Solving the optimization problem in Equation 4 is hard, as the number of integer variables in α equals the number of ReLU neurons in the neural network, which is typically very large. Therefore, we relax the problem by introducing a random variable π_{ij} indicating the categorical distribution of α_{ij} assigning to one of the three categories, where $\pi_{ij}^k \triangleq p(\alpha_{ij} = k)$ for $k = 1, 2, 3$. We can then reformulate the problem as:

$$\min_{\omega, \pi} \mathbb{E}[\mathcal{L}(\theta)] \quad \text{s.t.} \quad \sum_{i=1}^N \sum_{j=1}^{N_i} \pi_{ij}^1 \leq \varepsilon, \quad \alpha_{ij} \sim \pi_{ij}, \quad (5)$$

where $\pi \triangleq \{\pi_{ij} \mid i = 1, \dots, N, j = 1, \dots, N_i\}$.

In Equation 5, the sampling procedure $\alpha_{ij} \sim \pi_{ij}$ is not differentiable. In order to make end-to-end gradient-based optimization possible, we employ the Gumbel-Softmax [29, 50] technique to obtain a continuous approximation of the discrete distribution.

Specifically, for a 3-class categorical distribution π_{ij} , where the class probabilities are denoted as $\pi_{ij}^1, \pi_{ij}^2, \pi_{ij}^3$, Gumbel-Max [18] allows us to draw 3-dimensional one-hot categorical samples \hat{z}_{ij} from the distribution via:

$$\hat{z}_{ij} = \text{OneHot}(\arg \max_k (\log \pi_{ij}^k + g^k)), \quad (6)$$

where g^k are i.i.d. samples drawn from $\text{Gumbel}(0, 1)$, which is obtained by sampling $u^k \sim \text{Uniform}(0, 1)$ and computing $g^k = -\log(-\log(u^k))$. We can then use the softmax function as a continuous, differentiable approximation of the arg max function:

$$z_{ij}^k = \frac{\exp((\log \pi_{ij}^k + g^k)/\tau)}{\sum_{k'} \exp((\log \pi_{ij}^{k'} + g^{k'})/\tau)}. \quad (7)$$

We denote this operation as $z_{ij} \sim \text{Concrete}(\pi_{ij}, \tau)$ [50], where τ is a temperature parameter controlling how close the softmax approximation is to the discrete distribution. As the temperature τ approaches zero, samples from the Gumbel-Softmax distribution become one-hot and identical to the original categorical distribution.

After obtaining z_{ij} , we can calculate the activation value x_{ij}^+ as a weighted sum of different functional choices:

$$x_{ij}^+ = \hat{h}_{ij}(x_{ij}) \triangleq z_{ij}^1 \cdot \text{ReLU}(x_{ij}) + z_{ij}^2 \cdot \text{ID}(x_{ij}) + z_{ij}^3 \cdot \text{Zero}(x_{ij}), \quad (8)$$

and then use gradient descent to optimize both the weight parameters ω and the architecture distribution parameters π .

During training, we can also constrain z_{ij} to be one-hot vectors by using arg max, but use the continuous approximation in the backward pass by approximating $\nabla_{\theta} \hat{z}_{ij} \approx \nabla_{\theta} z_{ij}$. This is denoted as ‘‘Straight-Through’’ Gumbel Estimator in [29].

3.4 Optimization algorithm

Instead of limiting the number of regular ReLUs from the very beginning of the training process, we start with a randomly initialized neural network and use gradient descent to optimize ω and π by minimizing the following objective function until convergence:

$$\mathbb{E}[\mathcal{L}(\theta)] + \lambda R(\pi), \quad (9)$$

where the regularization term $R(\pi) \triangleq \sum_{i=1}^N \sum_{j=1}^{N_i} \pi_{ij}^1$ aims to explicitly reduce the use of the regular ReLU function. One could also consider adjusting it to $R(\pi) \triangleq \sum_{i=1}^N \sum_{j=1}^{N_i} (\pi_{ij}^1 + \lambda_{\text{ID}} \pi_{ij}^2)$ with a small λ_{ID} to discourage the use of identity mappings at the same time.

We then take an iterative approach by starting with a relatively large ε_1 and gradually decrease its value for K iterations with $\varepsilon_1 > \varepsilon_2 > \dots > \varepsilon_K = \varepsilon$. Within each optimization iteration using ε_k , we first rank the neurons according to $\max(\pi_{ij}^2, \pi_{ij}^3)$ in descending order, and assign the activation function for the top-ranked neurons as ID if $\pi_{ij}^2 \geq \pi_{ij}^3$, or Zero otherwise, while keeping the bottom ε_k neurons intact using Gumbel-Softmax as described in Section 3.3. Subsequently, we continue optimizing ω and π using gradient descent to minimize Equation 9. The sparsification process generates a range of models at various sparsification levels for subsequent investigations.

3.5 Closed-loop feedback control using the sparsified models

After we have obtained the sparsified dynamics models, we fix the model architecture and formulate the model-based planning task as the following trajectory optimization problem:

$$\min_u \sum_t c(y_t, u_t) \quad \text{s.t.} \quad y_{t+1} = \hat{f}_{\theta}(y_{t':t}, u_{t':t}), \quad (10)$$

where c is the cost function. When the transition function \hat{f}_{θ} is a highly nonlinear neural network, solving the optimization problem is not easy. Previous methods [77, 12, 60, 15, 51] typically regard the transition function as a black box and rely on sampling-based algorithms like the cross-entropy method (CEM) [61] and model-predictive path integral (MPPI) [73] for online planning. Others have also tried applying gradient descent to derive the action signals [39, 40]. However, the number of required samples grows exponentially with the number of inputs and trajectory length. Gradient descent can also be stuck in local optima, and it is also hard to assess the optimality or robustness of the derived action sequence using these methods.

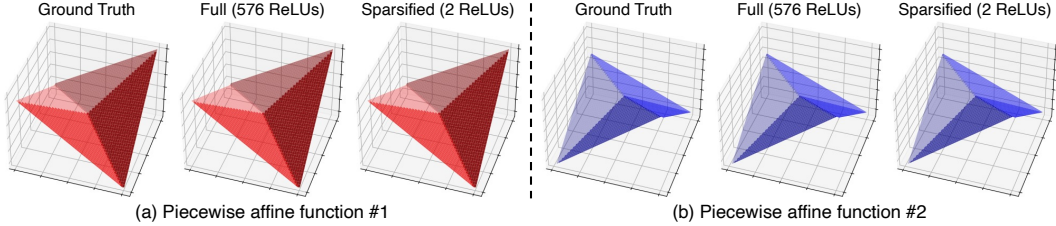


Figure 2: **Recover the ground truth piecewise affine functions from data.** We evaluate our sparsification pipeline on two hand-designed piecewise affine functions composed of four linear pieces. Our pipeline successfully generates sparsified models with 2 ReLUs that accurately fit the data, determine the region partition, and recover the underlying ground truth system.

3.5.1 Mixed-integer formulation of ReLU neural dynamics

The sparsified neural dynamics models open up the possibility of dissecting the model and solving the problem using more principled optimization tools. Specifically, given that a ReLU neural network is a piecewise affine function, we can formulate Equation 10 as MIP. We assign to each ReLU a binary variable $a = \mathbb{1}(x \geq 0)$ to indicate whether the pre-activation value is larger or smaller than zero. Given lower and upper bounds on the input $l \leq x \leq u$ (which we calculate by passing the offline dataset through the sparsified neural networks), the equality $x^+ = \text{ReLU}(x) \triangleq \max(0, x)$ can be modeled through the following set of mixed-integer linear constraints:

$$x^+ \leq x - l(1 - a), \quad x^+ \geq x, \quad x^+ \leq ua, \quad x^+ \geq 0, \quad a \in \{0, 1\}. \quad (11)$$

If only a few ReLUs are left in the model, Equation 10 can be efficiently solved to global optimality.

The formulation in Equation 11 is the simplest mixed-integer encoding of a ReLU network, and a variety of strategies are available in the literature to accelerate the solution of our MIPs. For large-scale models, it is possible to *warm start* the optimization process using sampling-based methods or gradient descent, and subsequently refine the solution using MIP solvers [53]. There also exist more advanced techniques to formulate the MIP [2, 52, 54], these can lead to tighter convex relaxations of our problem and allow us to identify high-quality solutions of Equation 10 earlier in the branch-and-bound process. The ability to find globally-optimal solutions is attractive but requires the model to exhibit a reasonable global performance. The sparsification step helps us also in this direction, since we typically expect a smaller simulation error from a sparsified (simpler) model than its unsparisified (very complicated) counterpart when moving away from the training distribution. In addition, we could also explicitly counteract this issue with the addition of trust-region constraints that prevent the optimizer from exploiting model inaccuracies in the areas of the input space that are not well-supported by the training data [56].

3.5.2 Tradeoff between model accuracy and closed-loop control performance

Models with fewer ReLUs are generally less accurate but permit the use of more advanced optimization tools, like efficient branch-and-bound algorithms implemented in state-of-the-art solvers. Within a model-predictive control (MPC) framework, the controller can leverage the environmental feedback to counteract prediction errors via online modifications of the action sequence. The iterative optimization procedure in Section 3.4 yields a series of models at different sparsification levels. By comparing their performances and investigating the trade-off between prediction accuracy and closed-loop control performance, we can select the model with the most desirable capacity.

4 Experiments

In our experiments, we seek to address three central questions: (1) How does the varying number of ReLUs affect the prediction accuracy? (2) How does the varying number of ReLUs affect open-loop planning? (3) Can the sparsified model, when combined with more principled optimization methods, deliver better closed-loop control results?

Environments, tasks, and model classes. We evaluate our framework on four environments specified in different observation spaces, including state, keypoints, and object-centric representations.

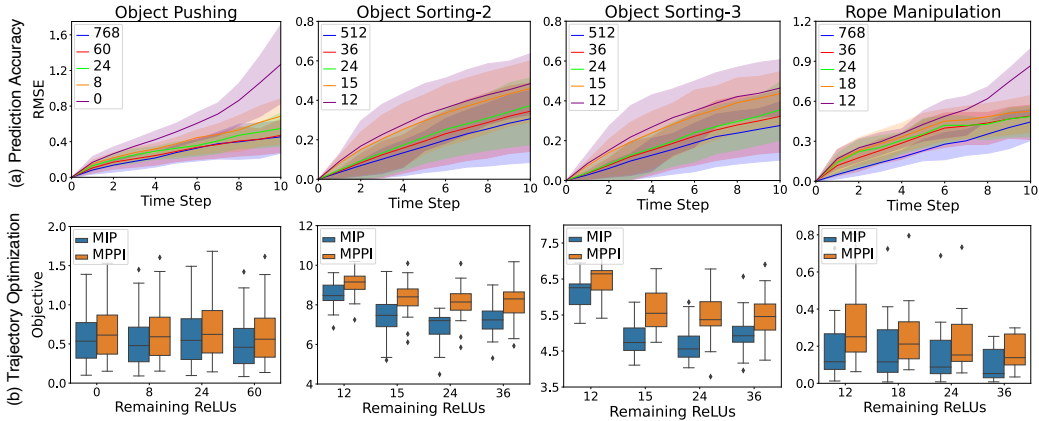


Figure 3: **Quantitative analysis of the sparsified models for open-loop prediction and planning.** (a) Long-term future prediction error, with the shaded area representing the region between the 25th and 75th percentiles. The significant overlap between the curves suggests that reducing the number of ReLUs only leads to a minimal decrease in prediction accuracy. (b) Results of the trajectory optimization problem from Equation 10. We compare two optimization formulations: mixed-integer programming (MIP) and model-predictive path integral (MPPI), using models with varying levels of sparsification. The figure clearly indicates that MIP consistently outperforms its sampling-based counterpart, MPPI.

These evaluation environments make use of different modeling classes, including vanilla MLPs and complex GNNs. For closed-loop control evaluation, we additionally present the performance of our framework on two standardized benchmark environments from OpenAI Gym [8], CartPole-v1 and Reacher-v4.

- **Piecewise affine function.** We consider manually designed two-dimensional piecewise affine functions consisting of four linear pieces (Figure 2), and the goal is to recover the ground-truth system from data through the sparsification process starting from an overparameterized MLP. To train the model, we collect 1,600 transition pairs from the ground truth functions uniformly distributed over the 2D input space.
- **Object pushing.** A fully-actuated pusher interacts with an object moving on a 2D plane, as depicted in Figure 4a. The goal is to manipulate the object to reach a randomly generated target pose. We generated 50,000 transition pairs using the Pymunk simulator [7]. The observation y_t is defined by the position of four selected keypoints on the object, and the dynamics model is also instantiated as an MLP.
- **Object sorting.** In Figure 4c, a pusher is used to sort a cluster of objects that lie on a table into corresponding target regions. In this environment, we generate a dataset consisting of 150,000 transition pairs with two objects using Pymunk. Following the success of previous graph-based dynamics models [4, 40, 39], we use GNNs as the model class. The model takes the object positions as input and allows compositional generalization to extrapolate settings containing more objects, supporting up to 8 objects as tested in our benchmark.
- **Rope manipulation.** Figure 4b shows the task of manipulating a deformable rope into a target shape. We generate a dataset of 60,000 transition pairs through random interactions using Nvidia FleX [49]. We use an MLP to model the dynamics, and the observation y_t is the position of four selected keypoints on the rope.

4.1 How does the varying number of ReLUs affect the prediction accuracy?

Recover the ground truth piecewise affine system from data. The sparsification procedure starts with the full model with four hidden layers and 576 ReLU units. It then undergoes seven iterations of sparsification, with the number of remaining ReLUs, represented as ε_k , diminishing from 25 down to 2. As illustrated in Figure 2, the sparsified model, which retains only two ReLUs, accurately identifies the region partition and achieves a nearly zero distance from the ground truth. This enables

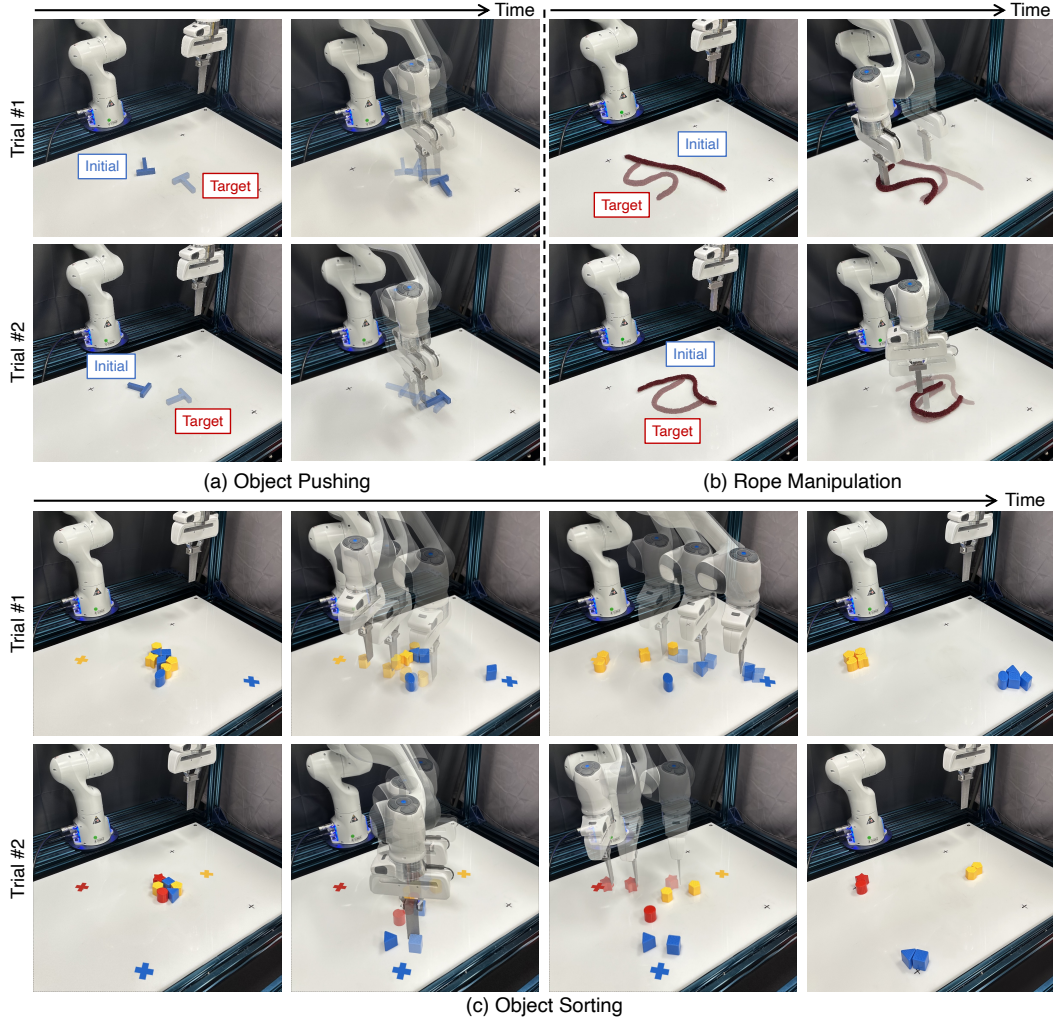


Figure 4: **Qualitative results on closed-loop feedback control.** (a) In object pushing, the objective is to manipulate the object to reach a randomly generated target pose, depicted as transparent in the first column. The second column illustrates how the planner, using the sparsified model, can leverage feedback from the environment to compensate for the modeling errors and accurately achieve the target. (b) The framework is also applicable to rope manipulation. Our sparsified model, in conjunction with the MIP formulation, facilitates closed-loop feedback control to manipulate the rope into desired configurations. (c) Our framework also consistently succeeds in object sorting tasks that involve complex contact events. Using the same model with the MIP formulation, the system can manipulate up to eight objects, sorting them into their respective regions.

the model to recover the underlying ground truth system and demonstrates the effectiveness of the sparsification procedure.

Future prediction using sparsified models at different sparsification levels. Existing literature provides comprehensive studies indicating that neural networks are overparameterized [23, 24, 17]. Still, we are interested in understanding how the proposed sparsification process affects the model prediction accuracy. We evaluate our framework on three benchmark environments, object pushing, sorting, and rope manipulation. Starting with the full model, we gradually sparsify it using decreasing values of ε_k . During training, we focus solely on the accuracy of one-step prediction but evaluate the models for their long-horizon predictive capability.

Figure 3a illustrates the prediction accuracy for models with varying numbers of ReLUs. “Object Sorting-2” denotes the task of sorting objects into two piles, while “Object Sorting-3” represents sorting into three piles. The blue curve shows the full-model performance, and the shaded area denotes the region between the 25th and 75th percentiles over 100 trials. The figure suggests that, even with significantly fewer ReLUs, the model still achieves a reasonable future prediction performance, with the confidence region significantly overlapping with that of the full model. It is worth

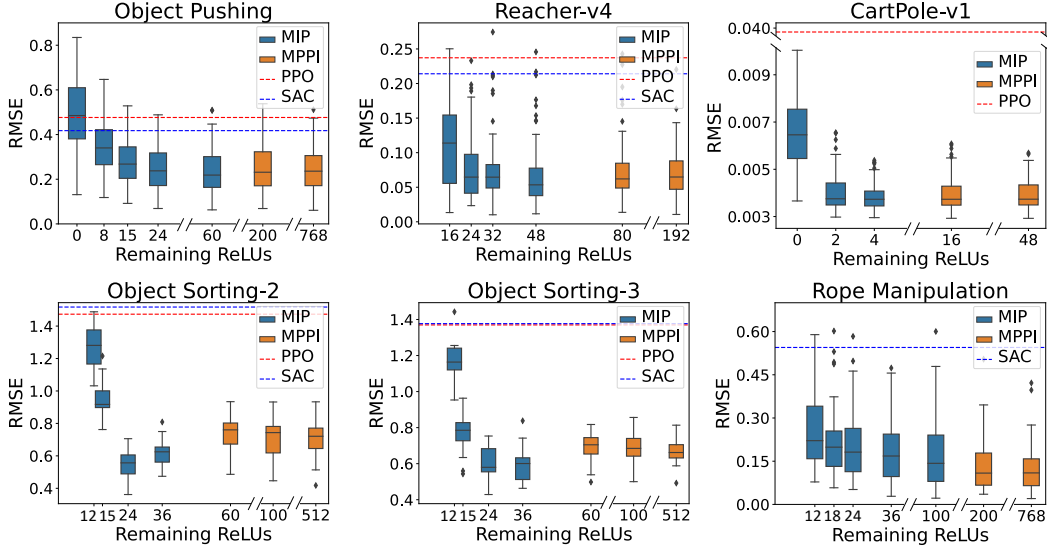


Figure 5: **Quantitative analysis of model sparsification vs. closed-loop control performance.** The horizontal axis represents the number of ReLUs remaining in the model, and the vertical axis indicates the closed-loop control performance. As shown in the figure, there exists a nice trade-off between the levels of model sparsification and the performance of closed-loop control. Models with fewer ReLUs are typically less accurate than the full model but make the MIP formulation tractable to solve. Across the spectrum of models, there exists a sweet spot, where a model, although only reasonably accurate, benefits from more powerful optimization tools and can lead to superior closed-loop control results. Moreover, our method consistently outperforms commonly used RL techniques such as PPO and SAC.[‡]

noting that our framework is adaptable to both vanilla MLPs (utilized in object pushing and rope manipulation) and GNNs (employed for object sorting), thereby showcasing the broad applicability of our proposed method. Later in Section 4.2 and 4.3, we will demonstrate that the sparsified models, although slightly less accurate than the full model, can yield superior open-loop and closed-loop optimization results when paired with more effective optimization tools.

4.2 How does the varying number of ReLUs affect open-loop planning?

Having obtained the sparsified models and examined their prediction accuracy, we next assess how these models can be applied to solve the trajectory optimization problem in Equation 10. The sparsified model contains significantly fewer ReLUs, making it feasible to use formulations with better optimality guarantees, as discussed in Section 3.5. Specifically, we formulate the optimization problem using MIP (Equation 11) and solve the problem using a commercial optimization solver, Gurobi [19]. We compare our method with MPPI, a commonly-used sampling-based alternative from the model-based RL community. As illustrated in Figure 3b, the MIP formulation permits the use of advanced branch-and-bound optimization procedures. With a sufficiently small number of ReLU units remaining in the neural dynamics models, we can solve the problem optimally. This consistently outperforms MPPI by a significant margin.

4.3 Can the sparsified model deliver better closed-loop control results?

The results in Section 4.2 only tell us how good different optimization procedures are as measured by the learned dynamics model. However, what we really care about is the performance when executing optimized plans in the original simulator or the real world. Therefore, it is crucial to evaluate the effectiveness of these models within a closed-loop control framework. Here we employ an MPC

[‡]We omit the result of PPO on rope manipulation due to compute limitations, because our rope simulator does not support accelerated-time simulation and takes excessively long before PPO gains reasonable performance. We omit the result of SAC on CartPole-v1 because the Stable Baselines 3 SAC implementation does not support a discrete action space.

framework that, taking into account the feedback from the environment, allows the agent to make online adjustments to the action sequence.

Figure 4 visualizes multiple execution trials of object pushing, sorting, and rope manipulation in the real world using our method. Our framework reliably pushes the object to its target pose, deforms the rope into the desired shape, and sorts the many objects into the corresponding piles. We then present the quantitative results for object pushing, sorting, and rope manipulation, along with two tasks from OpenAI Gym [8], *CartPole-v1* and *Reacher-v4*, measured in simulation, in Figure 5. Across various tasks, we observe a similar trade-off between the levels of model sparsification and closed-loop control performance. As the number of ReLUs decreases, there is typically a slight decrease in prediction accuracy, but as illustrated in Figure 5, this allows us to formulate the trajectory optimization problem as an MIP and solve it using efficient branch-and-bound algorithms. Consequently, within the spectrum of sparsified models, there exists an optimal point where a model, albeit only reasonably accurate, benefits from the more effective optimization tools and can result in better closed-loop control performance. Our iterative sparsification process, discussed in Section 3.4, enables us to easily identify such model. Furthermore, our method consistently outperforms commonly used RL techniques such as PPO [64] and SAC [20] when using the same number of interactions with the underlying environments.

5 Discussion

Conclusion. In this work, we propose to sparsify neural dynamics models for more effective closed-loop, model-based planning and control. Our formulation allows an end-to-end optimization of both the model class and the weight parameters. The sparsified models enable the use of efficient branch-and-bound algorithms and can deliver better performance in closed-loop control. Our framework applies to various dynamical systems and multiple neural network architectures, including vanilla MLPs and complicated GNNs. We also demonstrate the effectiveness and applicability of our method through its application to simple piecewise affine systems and manipulation tasks involving complex contact dynamics and deformable objects.

Our work draws inspiration and merges techniques from both the learning and control communities, which we hope can spur future investigations in this interdisciplinary direction to take advantage and make novel use of the powerful tools from both communities.

Limitations and future work. Our method relies on sparsifying neural dynamics models to fewer ReLU units to make the control optimization process solvable in a reasonable time due to the worst-case exponential run time of MIP solvers. Although our experiments showed that this already enabled us to complete a wide variety of tasks, our approach may struggle when facing a much larger neural dynamics model.

Our experiments also demonstrated superior closed-loop control performance using sparsified dynamics models with only reasonably good prediction accuracy as a result of benefiting from stronger optimization tools, but our approach may suffer if the sparsified dynamics model becomes significantly worse and incapable of providing useful forward predictions.

Acknowledgments. This work is in part supported by ONR MURI N00014-22-1-2740. Ziang Liu is supported by the Siebel Scholars program.

References

- [1] Pulkit Agrawal, Ashvin Nair, Pieter Abbeel, Jitendra Malik, and Sergey Levine. Learning to poke by poking: Experiential learning of intuitive physics. *arXiv preprint arXiv:1606.07419*, 2016.
- [2] Ross Anderson, Joey Huchette, Will Ma, Christian Tjandraatmadja, and Juan Pablo Vielma. Strong mixed-integer programming formulations for trained neural networks. *Mathematical Programming*, pages 1–37, 2020.
- [3] Sajid Anwar, Kyuyeon Hwang, and Wonyong Sung. Structured pruning of deep convolutional neural networks. *ACM Journal on Emerging Technologies in Computing Systems (JETC)*, 13(3):1–18, 2017.

- [4] Peter Battaglia, Razvan Pascanu, Matthew Lai, Danilo Jimenez Rezende, et al. Interaction networks for learning about objects, relations and physics. *Advances in neural information processing systems*, 29, 2016.
- [5] Paul J. Besl and Neil D. McKay. A method for registration of 3-d shapes. *IEEE Trans. Pattern Anal. Mach. Intell.*, 14:239–256, 1992.
- [6] Davis Blalock, Jose Javier Gonzalez Ortiz, Jonathan Frankle, and John Gutttag. What is the state of neural network pruning? *arXiv preprint arXiv:2003.03033*, 2020.
- [7] Victor Blomqvist. Pymunk. <https://pymunk.org>, November 2022. Version 6.4.0.
- [8] Greg Brockman, Vicki Cheung, Ludwig Pettersson, Jonas Schneider, John Schulman, Jie Tang, and Wojciech Zaremba. Openai gym. *CoRR*, abs/1606.01540, 2016. URL <http://arxiv.org/abs/1606.01540>.
- [9] Han Cai, Ligeng Zhu, and Song Han. Proxylessnas: Direct neural architecture search on target task and hardware. *arXiv preprint arXiv:1812.00332*, 2018.
- [10] Marc Deisenroth and Carl E Rasmussen. Pilco: A model-based and data-efficient approach to policy search. In *Proceedings of the 28th International Conference on machine learning (ICML-11)*, pages 465–472. Citeseer, 2011.
- [11] James K Doyle and David N Ford. Mental models concepts for system dynamics research. *System dynamics review: the journal of the System Dynamics Society*, 14(1):3–29, 1998.
- [12] Frederik Ebert, Chelsea Finn, Alex X Lee, and Sergey Levine. Self-supervised visual planning with temporal skip connections. In *CoRL*, pages 344–356, 2017.
- [13] Frederik Ebert, Chelsea Finn, Sudeep Dasari, Annie Xie, Alex Lee, and Sergey Levine. Visual foresight: Model-based deep reinforcement learning for vision-based robotic control. *arXiv preprint arXiv:1812.00568*, 2018.
- [14] Thomas Elsken, Jan Hendrik Metzen, Frank Hutter, et al. Neural architecture search: A survey. *J. Mach. Learn. Res.*, 20(55):1–21, 2019.
- [15] Chelsea Finn and Sergey Levine. Deep visual foresight for planning robot motion. In *2017 IEEE International Conference on Robotics and Automation (ICRA)*, pages 2786–2793. IEEE, 2017.
- [16] Chelsea Finn, Ian Goodfellow, and Sergey Levine. Unsupervised learning for physical interaction through video prediction. *arXiv preprint arXiv:1605.07157*, 2016.
- [17] Jonathan Frankle and Michael Carbin. The lottery ticket hypothesis: Finding sparse, trainable neural networks. *arXiv preprint arXiv:1803.03635*, 2018.
- [18] Emil Julius Gumbel. *Statistical theory of extreme values and some practical applications: a series of lectures*, volume 33. US Government Printing Office, 1954.
- [19] Gurobi Optimization, LLC. Gurobi Optimizer Reference Manual, 2023. URL <https://www.gurobi.com>.
- [20] Tuomas Haarnoja, Aurick Zhou, Pieter Abbeel, and Sergey Levine. Soft actor-critic: Off-policy maximum entropy deep reinforcement learning with a stochastic actor. In *International conference on machine learning*, pages 1861–1870. PMLR, 2018.
- [21] Danijar Hafner, Timothy Lillicrap, Jimmy Ba, and Mohammad Norouzi. Dream to control: Learning behaviors by latent imagination. *arXiv preprint arXiv:1912.01603*, 2019.
- [22] Danijar Hafner, Timothy Lillicrap, Ian Fischer, Ruben Villegas, David Ha, Honglak Lee, and James Davidson. Learning latent dynamics for planning from pixels. In *International Conference on Machine Learning*, pages 2555–2565. PMLR, 2019.

- [23] Song Han, Huizi Mao, and William J Dally. Deep compression: Compressing deep neural networks with pruning, trained quantization and huffman coding. *arXiv preprint arXiv:1510.00149*, 2015.
- [24] Song Han, Jeff Pool, John Tran, and William Dally. Learning both weights and connections for efficient neural network. *Advances in neural information processing systems*, 28, 2015.
- [25] Yihui He, Xiangyu Zhang, and Jian Sun. Channel pruning for accelerating very deep neural networks. In *Proceedings of the IEEE international conference on computer vision*, pages 1389–1397, 2017.
- [26] Arthur J Helmicki, Clas A Jacobson, and Carl N Nett. Control oriented system identification: a worst-case/deterministic approach in h/sub infinity. *IEEE Transactions on Automatic control*, 36(10):1163–1176, 1991.
- [27] François Robert Hogan and Alberto Rodriguez. Feedback control of the pusher-slider system: A story of hybrid and underactuated contact dynamics. *arXiv preprint arXiv:1611.08268*, 2016.
- [28] Zixuan Huang, Xingyu Lin, and David Held. Mesh-based dynamics model with occlusion reasoning for cloth manipulation. In *Robotics: Science and Systems (RSS)*, 2022.
- [29] Eric Jang, Shixiang Gu, and Ben Poole. Categorical reparameterization with gumbel-softmax. *arXiv preprint arXiv:1611.01144*, 2016.
- [30] Michael Janner, Justin Fu, Marvin Zhang, and Sergey Levine. When to trust your model: Model-based policy optimization. *CoRR*, abs/1906.08253, 2019. URL <http://arxiv.org/abs/1906.08253>.
- [31] Natalie A Jones, Helen Ross, Timothy Lynam, Pascal Perez, and Anne Leitch. Mental models: an interdisciplinary synthesis of theory and methods. *Ecology and Society*, 16(1), 2011.
- [32] Diederik P. Kingma and Jimmy Ba. Adam: A method for stochastic optimization. In Yoshua Bengio and Yann LeCun, editors, *3rd International Conference on Learning Representations, ICLR 2015, San Diego, CA, USA, May 7-9, 2015, Conference Track Proceedings*, 2015. URL <http://arxiv.org/abs/1412.6980>.
- [33] Alexander Kirillov, Eric Mintun, Nikhila Ravi, Hanzi Mao, Chloe Rolland, Laura Gustafson, Tete Xiao, Spencer Whitehead, Alexander C. Berg, Wan-Yen Lo, Piotr Dollár, and Ross Girshick. Segment anything. *arXiv:2304.02643*, 2023.
- [34] Tejas D Kulkarni, Ankush Gupta, Catalin Ionescu, Sebastian Borgeaud, Malcolm Reynolds, Andrew Zisserman, and Volodymyr Mnih. Unsupervised learning of object keypoints for perception and control. *Advances in neural information processing systems*, 32:10724–10734, 2019.
- [35] Brenden M Lake, Tomer D Ullman, Joshua B Tenenbaum, and Samuel J Gershman. Building machines that learn and think like people. *Behavioral and brain sciences*, 40, 2017.
- [36] Yann LeCun, John S Denker, and Sara A Solla. Optimal brain damage. In *Advances in neural information processing systems*, pages 598–605, 1990.
- [37] Joonho Lee, Jemin Hwangbo, Lorenz Wellhausen, Vladlen Koltun, and Marco Hutter. Learning quadrupedal locomotion over challenging terrain. *Science robotics*, 5(47), 2020.
- [38] Hao Li, Asim Kadav, Igor Durdanovic, Hanan Samet, and Hans Peter Graf. Pruning filters for efficient convnets. *arXiv preprint arXiv:1608.08710*, 2016.
- [39] Yunzhu Li, Jiajun Wu, Russ Tedrake, Joshua B Tenenbaum, and Antonio Torralba. Learning particle dynamics for manipulating rigid bodies, deformable objects, and fluids. *arXiv preprint arXiv:1810.01566*, 2018.
- [40] Yunzhu Li, Jiajun Wu, Jun-Yan Zhu, Joshua B Tenenbaum, Antonio Torralba, and Russ Tedrake. Propagation networks for model-based control under partial observation. In *2019 International Conference on Robotics and Automation (ICRA)*, pages 1205–1211. IEEE, 2019.

- [41] Yunzhu Li, Hao He, Jiajun Wu, Dina Katabi, and Antonio Torralba. Learning compositional koopman operators for model-based control. In *International Conference on Learning Representations*, 2020. URL <https://openreview.net/forum?id=H1ldzA4tPr>.
- [42] Yunzhu Li, Antonio Torralba, Anima Anandkumar, Dieter Fox, and Animesh Garg. Causal discovery in physical systems from videos. *Advances in Neural Information Processing Systems*, 33, 2020.
- [43] Chenxi Liu, Barret Zoph, Maxim Neumann, Jonathon Shlens, Wei Hua, Li-Jia Li, Li Fei-Fei, Alan Yuille, Jonathan Huang, and Kevin Murphy. Progressive neural architecture search. In *Proceedings of the European conference on computer vision (ECCV)*, pages 19–34, 2018.
- [44] Hanxiao Liu, Karen Simonyan, and Yiming Yang. Darts: Differentiable architecture search. *arXiv preprint arXiv:1806.09055*, 2018.
- [45] Shilong Liu, Zhaoyang Zeng, Tianhe Ren, Feng Li, Hao Zhang, Jie Yang, Chunyuan Li, Jianwei Yang, Hang Su, Jun Zhu, and Lei Zhang. Grounding dino: Marrying dino with grounded pre-training for open-set object detection, 2023.
- [46] Zechun Liu, Haoyuan Mu, Xiangyu Zhang, Zichao Guo, Xin Yang, Kwang-Ting Cheng, and Jian Sun. Metapruning: Meta learning for automatic neural network channel pruning. In *Proceedings of the IEEE/CVF international conference on computer vision*, pages 3296–3305, 2019.
- [47] Zhuang Liu, Jianguo Li, Zhiqiang Shen, Gao Huang, Shoumeng Yan, and Changshui Zhang. Learning efficient convolutional networks through network slimming. In *Proceedings of the IEEE international conference on computer vision*, pages 2736–2744, 2017.
- [48] Lennart Ljung. *System identification*. Springer, 1998.
- [49] Miles Macklin, Matthias Müller, Nuttapon Chentanez, and Tae-Yong Kim. Unified particle physics for real-time applications. *ACM Transactions on Graphics (TOG)*, 33(4):1–12, 2014.
- [50] Chris J Maddison, Andriy Mnih, and Yee Whye Teh. The concrete distribution: A continuous relaxation of discrete random variables. *arXiv preprint arXiv:1611.00712*, 2016.
- [51] Lucas Manuelli, Yunzhu Li, Pete Florence, and Russ Tedrake. Keypoints into the future: Self-supervised correspondence in model-based reinforcement learning. *arXiv preprint arXiv:2009.05085*, 2020.
- [52] Tobia Marcucci and Russ Tedrake. Mixed-integer formulations for optimal control of piecewise-affine systems. In *Proceedings of the 22nd ACM International Conference on Hybrid Systems: Computation and Control*, pages 230–239, 2019.
- [53] Tobia Marcucci and Russ Tedrake. Warm start of mixed-integer programs for model predictive control of hybrid systems. *IEEE Transactions on Automatic Control*, 2020.
- [54] Tobia Marcucci, Jack Umenberger, Pablo A Parrilo, and Russ Tedrake. Shortest paths in graphs of convex sets. *arXiv preprint arXiv:2101.11565*, 2021.
- [55] Microsoft. Neural Network Intelligence, 1 2021. URL <https://github.com/microsoft/nni>.
- [56] Peter Mitrano, Dale McConachie, and Dmitry Berenson. Learning where to trust unreliable models in an unstructured world for deformable object manipulation. *Science Robotics*, 6(54): eabd8170, 2021.
- [57] Thomas M Moerland, Joost Broekens, and Catholijn M Jonker. Model-based reinforcement learning: A survey. *arXiv preprint arXiv:2006.16712*, 2020.
- [58] Pavlo Molchanov, Stephen Tyree, Tero Karras, Timo Aila, and Jan Kautz. Pruning convolutional neural networks for resource efficient inference. *arXiv preprint arXiv:1611.06440*, 2016.

- [59] Bruce Moore. Principal component analysis in linear systems: Controllability, observability, and model reduction. *IEEE transactions on automatic control*, 26(1):17–32, 1981.
- [60] Anusha Nagabandi, Kurt Konolige, Sergey Levine, and Vikash Kumar. Deep dynamics models for learning dexterous manipulation. In *Conference on Robot Learning*, pages 1101–1112. PMLR, 2020.
- [61] Reuven Y Rubinfeld and Dirk P Kroese. *The cross-entropy method: a unified approach to combinatorial optimization, Monte-Carlo simulation and machine learning*. Springer Science & Business Media, 2013.
- [62] Alvaro Sanchez-Gonzalez, Nicolas Heess, Jost Tobias Springenberg, Josh Merel, Martin A. Riedmiller, Raia Hadsell, and Peter W. Battaglia. Graph networks as learnable physics engines for inference and control. *CoRR*, abs/1806.01242, 2018. URL <http://arxiv.org/abs/1806.01242>.
- [63] Julian Schrittwieser, Ioannis Antonoglou, Thomas Hubert, Karen Simonyan, Laurent Sifre, Simon Schmitt, Arthur Guez, Edward Lockhart, Demis Hassabis, Thore Graepel, et al. Mastering atari, go, chess and shogi by planning with a learned model. *Nature*, 588(7839):604–609, 2020.
- [64] John Schulman, Filip Wolski, Prafulla Dhariwal, Alec Radford, and Oleg Klimov. Proximal policy optimization algorithms. *arXiv preprint arXiv:1707.06347*, 2017.
- [65] Haochen Shi, Huazhe Xu, Zhiao Huang, Yunzhu Li, and Jiajun Wu. Robocraft: Learning to see, simulate, and shape elasto-plastic objects with graph networks. *arXiv preprint arXiv:2205.02909*, 2022.
- [66] Kin Cheong Sou, Alexandre Megretski, and Luca Daniel. A quasi-convex optimization approach to parameterized model order reduction. In *Proceedings of the 42nd annual Design Automation Conference*, pages 933–938, 2005.
- [67] HJ Suh and Russ Tedrake. The surprising effectiveness of linear models for visual foresight in object pile manipulation. *arXiv preprint arXiv:2002.09093*, 2020.
- [68] Vincent Tjeng, Kai Xiao, and Russ Tedrake. Evaluating robustness of neural networks with mixed integer programming. *arXiv preprint arXiv:1711.07356*, 2017.
- [69] Tianzhe Wang, Kuan Wang, Han Cai, Ji Lin, Zhijian Liu, Hanrui Wang, Yujun Lin, and Song Han. Apq: Joint search for network architecture, pruning and quantization policy. In *Proceedings of the IEEE/CVF Conference on Computer Vision and Pattern Recognition*, pages 2078–2087, 2020.
- [70] Manuel Watter, Jost Tobias Springenberg, Joschka Boedecker, and Martin Riedmiller. Embed to control: A locally linear latent dynamics model for control from raw images. *arXiv preprint arXiv:1506.07365*, 2015.
- [71] Tianhao Wei and Changliu Liu. Safe control with neural network dynamic models. In Roya Firoozi, Negar Mehr, Eren Yel, Rika Antonova, Jeannette Bohg, Mac Schwager, and Mykel Kochenderfer, editors, *Proceedings of The 4th Annual Learning for Dynamics and Control Conference*, volume 168 of *Proceedings of Machine Learning Research*, pages 739–750. PMLR, 23–24 Jun 2022. URL <https://proceedings.mlr.press/v168/wei22a.html>.
- [72] Wei Wen, Chunpeng Wu, Yandan Wang, Yiran Chen, and Hai Li. Learning structured sparsity in deep neural networks. *arXiv preprint arXiv:1608.03665*, 2016.
- [73] Grady Williams, Andrew Aldrich, and Evangelos A Theodorou. Model predictive path integral control: From theory to parallel computation. *Journal of Guidance, Control, and Dynamics*, 40(2):344–357, 2017.
- [74] Bichen Wu, Xiaoliang Dai, Peizhao Zhang, Yanghan Wang, Fei Sun, Yiming Wu, Yuandong Tian, Peter Vajda, Yangqing Jia, and Kurt Keutzer. Fbnet: Hardware-aware efficient convnet design via differentiable neural architecture search. In *Proceedings of the IEEE/CVF Conference on Computer Vision and Pattern Recognition*, pages 10734–10742, 2019.

- [75] Philipp Wu, Alejandro Escontrela, Danijar Hafner, Pieter Abbeel, and Ken Goldberg. Daydreamer: World models for physical robot learning. In *Conference on Robot Learning*, pages 2226–2240. PMLR, 2023.
- [76] Kai Y Xiao, Vincent Tjeng, Nur Muhammad Shafiullah, and Aleksander Madry. Training for faster adversarial robustness verification via inducing relu stability. *arXiv preprint arXiv:1809.03008*, 2018.
- [77] Lin Yen-Chen, Maria Bauza, and Phillip Isola. Experience-embedded visual foresight. In *Conference on Robot Learning*, pages 1015–1024. PMLR, 2020.
- [78] Aojun Zhou, Yukun Ma, Junnan Zhu, Jianbo Liu, Zhijie Zhang, Kun Yuan, Wenxiu Sun, and Hongsheng Li. Learning n: M fine-grained structured sparse neural networks from scratch. *arXiv preprint arXiv:2102.04010*, 2021.
- [79] Jiaji Zhou, Yifan Hou, and Matthew T Mason. Pushing revisited: Differential flatness, trajectory planning, and stabilization. *The International Journal of Robotics Research*, 38(12-13): 1477–1489, 2019.
- [80] Barret Zoph and Quoc V Le. Neural architecture search with reinforcement learning. *arXiv preprint arXiv:1611.01578*, 2016.

A How does our method compare to prior works in model-based RL?

In this experiment, we aim to examine how the closed-loop control performance of our method compare to prior works in model-based reinforcement learning, evaluated on standard benchmark environments. We conduct experiments on two additional tasks from OpenAI Gym [8], `CartPole-v1` and `Reacher-v4`, following the same procedures as described in Section 4.3. On top of a sampling-based planner (MPPI) and a model-free RL method (PPO), we employ two additional model-based RL methods, (1) using PPO to learn a control policy from our learned full neural dynamics model, and (2) MBPO [30] learning a model and a policy from scratch. The model-based RL methods require additional time to train a policy using the learned dynamics model, whereas our approach directly optimizes a task objective over the dynamics model without needing additional training.

The experiment results shown in Figure 6 further demonstrate the superior performance of our approach compared to prior methods on the two standard benchmark tasks. Notably, our approach achieves better performance with highly sparsified neural dynamics models with fewer ReLUs compared to prior works.

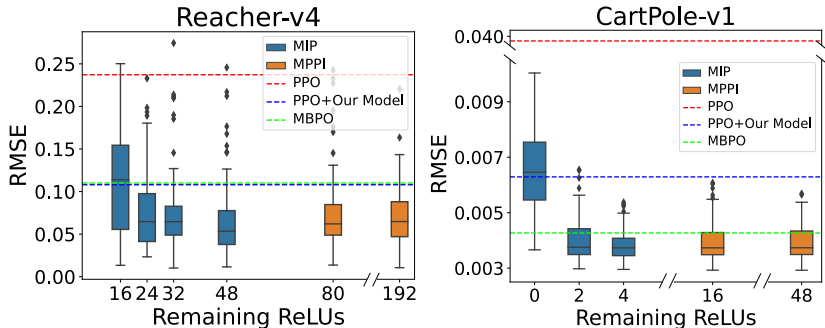


Figure 6: Closed-loop control performance of our method (MIP) compared against prior methods on two new environments. Our method with fewer ReLUs outperforms prior methods using models with more ReLUs, and we similarly observe a sweet spot that balances between model prediction accuracy and control performance.

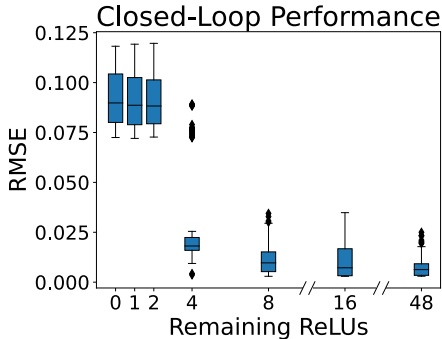


Figure 7: We tested the closed-loop control performance of dynamics models trained and simplified using our method by incorporating them as the forward model in a model-based RL framework optimized with PPO. Our findings indicate that even when the dynamics models are substantially simplified, they continue to allow for satisfactory control performance.

B Do models trained using our approach generalize to prior model-based RL methods?

The neural dynamics model learned in our method is generic and not limited to only working with our planning framework. We take the learned full and sparsified dynamics models on the `CartPole-v1` environment and train a control policy with PPO interacting only with the learned model, and provide the experiment results in Figure 7.

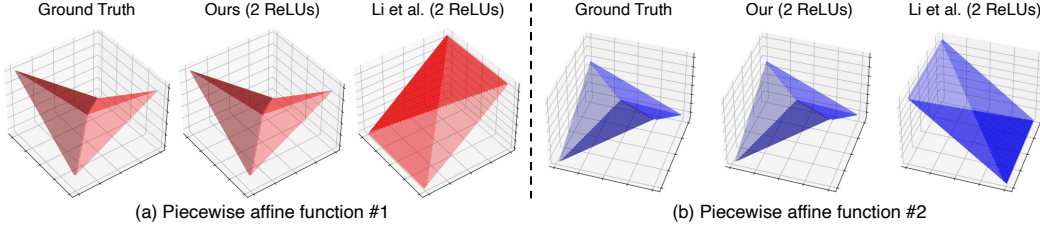


Figure 8: **Comparison with the channel pruning baseline on recovering the PWA functions.** We evaluate both our sparsification pipeline and the channel pruning baseline using two hand-designed piecewise affine functions, each composed of four linear pieces. Our pipeline successfully recovers the underlying ground truth system, whereas the baseline does not provide an accurate match.

The results show that the neural dynamics models trained in our method can generalize and combine with another model-based control framework. As the model becomes progressively sparsified, the closed-loop control performance gracefully degrades.

C How does our sparsification technique compare to prior neural network pruning methods?

The aim of this study is to discuss and compare our sparsification technique with the pruning methods commonly employed in the field. Most pruning strategies in existing literature primarily focus on eliminating as many *neurons* as possible to reduce computation and enhance efficiency. In contrast, our method aims to eliminate as many *nonlinearities* from the neural networks as possible. This differs from channel pruning, which only zeroes out values. Our approach permits the replacement of ReLU activations with identity mappings, the inclusion of which allows a more accurate model to be achieved at an equivalent level of sparsification. This offers a considerable advantage during the planning stage.

To illustrate our point more concretely, we provide, in this section, experimental results comparing our method against Level 1 Channel Pruning as referenced in [38].

C.1 Evaluation on Piecewise Affine (PWA) Functions

The two pruning methods are tasked to recover the ground truth PWA functions, as detailed in the experiment section of the main paper. Figure 8 illustrates the results after sparsifying the neural networks to two rectified linear units (ReLU) using both methods. Our method successfully identifies the region partition and the correct equations for describing values of each region, whereas the baseline [38] exhibits noticeable deviations.

C.2 Evaluation on Dynamics Prediction

In this section, we extend the comparison to three other tasks: object pushing, object sorting, and rope manipulation. For the object pushing and rope manipulation tasks, we train the neural dynamics model for a defined number of epochs before pruning is carried out by masking particular channels. Post-pruning, model speedup is performed using Neural Network Intelligence Library [55] to alter the model’s architecture and remove masked neurons. This process is repeated as further channels are pruned and the models are finetuned for additional epochs.

For the object sorting task involving graph neural networks, we perform a similar procedure to construct the baseline. During the initial model training phase, the mask resulting from the L_1 norm pruning operation is used to nullify specific weights, and the corresponding gradients are also masked during the finetuning phase.

To ensure fairness and reliability in the comparison, we maintain identical settings for both our sparsification technique and the pruning baseline. Therefore, for every round of compression, both models are subjected to the same number of training epochs, using the same dataset, and are reduced to the same number of ReLU units.

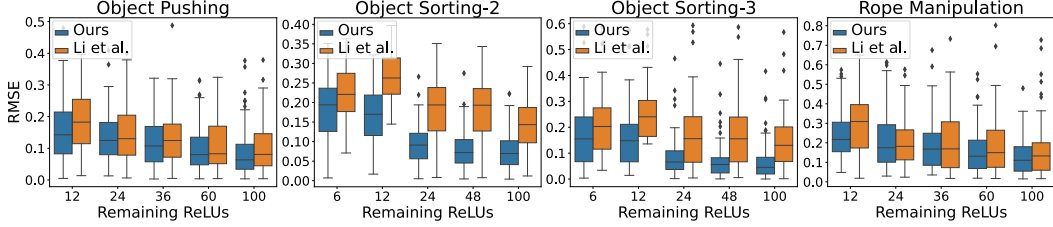


Figure 9: **Dynamics prediction error of sparsified models using our method vs. baseline.** We compare the dynamics prediction error of models sparsified using our method against models sparsified using the channel pruning method proposed by Li et al. [38]. The x-axis represents the number of remaining ReLU units in the model. The y-axis represents the prediction error measured by the root mean squared error between the prediction and the ground truth next state. Because our sparsification method only targets non-linear units while allowing linear units, models sparsified using our method constantly exhibit lower prediction error across all task settings.

We provide quantitative comparisons between our sparsification method and the baseline in Figure 9. Throughout the sparsification process, because our sparsification objective allows replacing non-linearities with identity mappings, our method consistently achieves a superior performance measured by prediction error, across all tasks.

C.3 Evaluation on Closed-Loop Control

In this experiment, we aim to further examine whether our method also boosts the closed-loop control performance that is critical for executing the optimized plans in the real world. We choose the object pushing task, and prune the learned dynamics model down to 36, 24, 18, and 15 ReLU units using our proposed sparsification method and the channel pruning method proposed by Li et al. [38] respectively. As shown in Figure 10, models pruned using our method consistently exhibit superior closed-loop control performance across all sparsification levels.

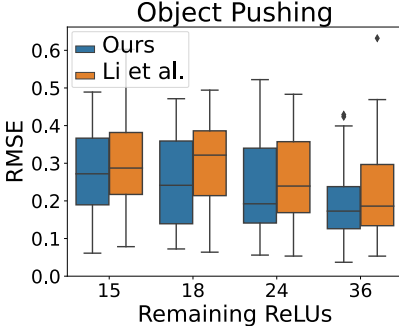


Figure 10: An ablation of our sparsification method compared with a prior network pruning method, evaluated by closed-loop control performance, demonstrating superior performance in closed-loop control.

D Experiment Details

D.1 Perception

We use a single top-down RealSense D435i camera to capture color and depth images of the workspace (Figure 11). The color image is segmented using state-of-the-art detection and segmentation models, Grounding DINO [45] and Segment Anything Model (SAM) [33]. Given a prompt, Grounding DINO generates a bounding box for the corresponding objects in the image. To minimize detection errors, we implement specific thresholds for confidence and bounding box area for different prompts. The resulting bounding box coordinates are then utilized by SAM to produce an instance mask for the corresponding object. The mask, along with the depth image, camera intrinsics and extrinsics, are used to calculate the position of all segmented points in the global frame.

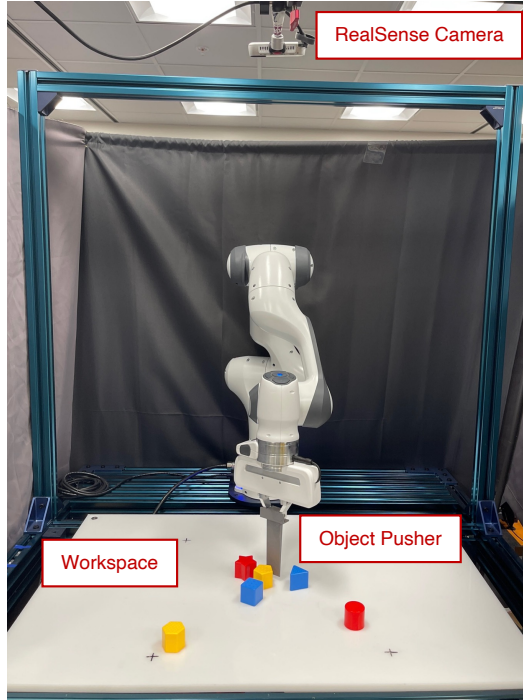


Figure 11: **Robot hardware experiments setup.** Robot experiments setup with a Franka Emika 7-DOF Panda robot arm and a top-down RealSense D435i RGB-D camera.

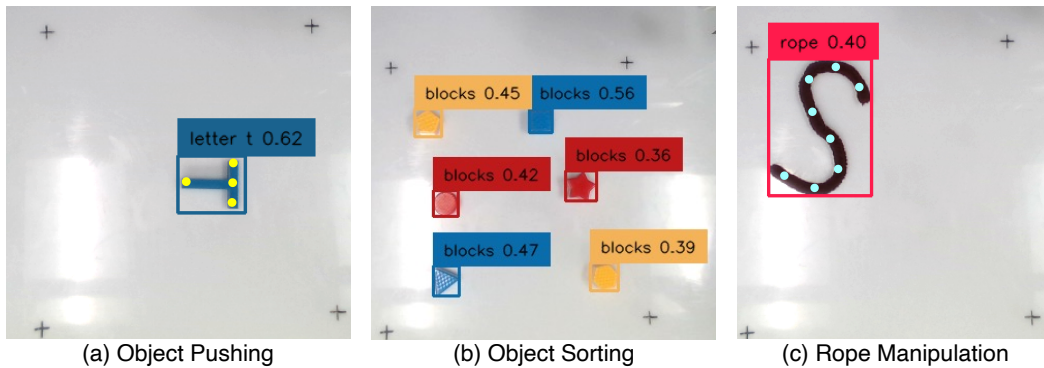


Figure 12: **Object and keypoint detection examples from our perception pipeline.** (a) Bounding box and detected keypoints positions. (b) Instance bounding boxes and detected object color. (c) Evenly spaced keypoints detected on the rope segment.

D.2 PWA Functions

We test our sparsification algorithm on recovering simple PWA functions, with two arguments and four affine pieces. The training data contains 1.6×10^3 transition pairs uniformly sampled within the input space with the ground truth function.

Our sparsification method starts with a Multi-Layer Perceptron (MLP) with $[96, 192, 192, 96]$ units in each layer and aggressively sparsifies into a compact model with only 2 ReLU units. We train using an Adam optimizer [32] with a learning rate of 1×10^{-4} until convergence, then finetune for 6×10^3 epochs in each sparsification round to obtain the final model.

D.3 Object Pushing

We provide a task-specific prompt “letter t” to the perception module along with confidence and bounding box thresholds to retrieve the bounding box around the T-shaped object (Figure 12a). After obtaining the segmentation mask of the object within the bounding box from SAM, we apply the

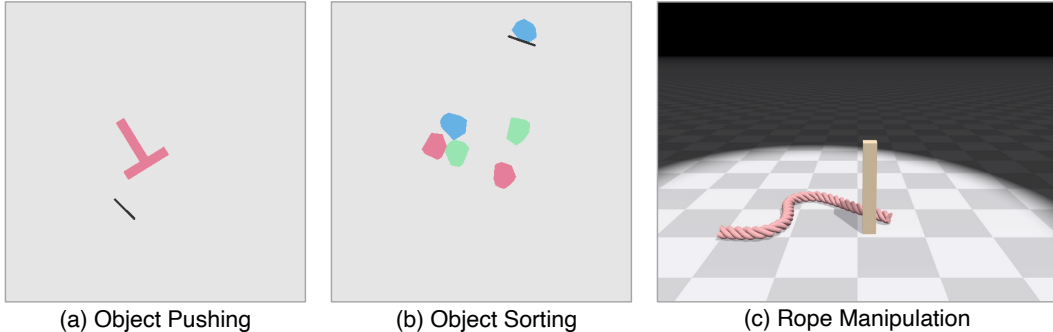


Figure 13: **Simulation environments used for data collection.** (a) The T-shaped object (pink) and the pusher (black) implemented in Pymunk for the object pushing task. (b) Objects of different colors interacting with the pusher (black) for the object sorting task. (c) The rope (pink) and the pusher (yellow) for the rope manipulation task, implemented with PyFleX [39].

mask to the depth image captured by the top-down camera to select only the subset of the pointcloud on the object. The position and orientation of the T-shaped object is determined by registering the captured pointcloud against a reference pointcloud sampled from a mesh model, using the Iterative Closest Points method [5].

The goal of the object pushing task is to position and orient a T-shaped object to align with a randomly sampled configuration within the workspace. Each action is a straight push from a start position to an end position. The state of the object at each time step is described with an ordered list of the coordinates of four selected keypoints. The dataset contains 5×10^4 transition pairs collected using the Pymunk simulator [7] (Figure 13a). To train our dynamics model, we concatenate the current keypoint state with the action, and pass through a three-layer MLP with 256 hidden units in each layer. We supervise the training with the mean squared error between the predicted next state \hat{y} and the ground truth state y from executing the given action in the current state in the simulator, accompanied with an L_1 and L_2 weight regularization term and both ReLU and ID regularization terms as described in Section 3.4 of the main paper.

The full loss is defined as

$$\mathcal{L} = \text{MSE}(y, \hat{y}) + \lambda_{\text{ReLU}}\pi^1 + \lambda_{\text{ID}}\pi^2 + \lambda_{\text{reg}}(R_{L_1} + R_{L_2}), \quad (12)$$

where $\lambda_{\text{ReLU}} = 2 \times 10^{-3}$, $\lambda_{\text{ID}} = 1 \times 10^{-4}$, and $\lambda_{\text{reg}} = 3 \times 10^{-4}$ are constants balancing between the loss terms, selected for each task based on empirical performance on dynamics prediction. The sparsification process starts with the full model with 768 ReLUs and gradually reduces to 0 ReLUs (linear model), trained with an Adam optimizer [32] with a learning rate of 5×10^{-4} . We train the full model until convergence, then train each of the sparsified models for 400 epochs.

We formulate the closed-loop feedback control problem with the sparsified models following Section 3.5, and optimize for the objective to minimize the squared L_2 distance between the predicted state \hat{y} by the dynamics model and the goal state y^* .

Our dynamics models are trained with one NVIDIA GeForce RTX 2080 Ti or one NVIDIA TITAN RTX GPU, followed by closed-loop control optimization using Gurobi [19] on an Intel i7-7700K 4.2 GHz CPU.

D.4 Object Sorting

In the object sorting task, we initialize the environment with two or more randomly placed objects of two to three different colors. The goal is to collect objects of the same color near a distinctive goal region for each color. We experiment with six task variations, with two colors, one to four objects each color, or three colors, one or two objects each. The actions are specified by the start and end locations, similar to the object pushing task.

For perception, we prompt Grounding DINO with “blocks”, then use the returned bounding boxes to obtain instance segmentation masks from SAM (Figure 12b). The position of each object is

calculated as the centroid of the positions of all points captured by the segmentation mask. The color of each object is determined based on the average color of all pixels captured by the mask.

To demonstrate the applicability of our method on more complex neural dynamics models, and due to the permutation-invariant nature of the task, we choose graph neural networks as the function class. We adapt a model architecture similar to what was employed by Sanchez-Gonzalez et al. [62] with 64 hidden units per layer, and train with an Adam optimizer [32] using a learning rate of 1×10^{-3} . The loss function is the mean squared error between the predicted next state for all objects and the ground truth state, coupled with regularization terms as described in Equation 12, with $\lambda_{\text{ReLU}} = 3 \times 10^{-4}$, $\lambda_{\text{ID}} = 3 \times 10^{-5}$, and $\lambda_{\text{reg}} = 1 \times 10^{-4}$. The full model with 512 ReLUs is trained until convergence on a dataset with 1.5×10^5 transitions involving random interactions with only two objects collected in Pymunk [7] (Figure 13b), and each sparsified model is trained for 100 epochs.

The closed-loop control optimization is formulated using the same sparsified model for all task variations. We calculated the squared L_2 distance between each object and the goal of the corresponding color, and use the summation of all individual object-goal distances as the optimization objective.

D.5 Rope Manipulation

We use a prompt of “rope” for the rope manipulation task. Detecting the pose of keypoints on the deformable rope requires an additional step in the perception module. After generating a segmentation mask using SAM, we use Singular Value Decomposition to find the vector that approximately divides the rope mask into two segments of equal length, then recursively bisects each segment until we obtain eight segments of similar lengths. The keypoints are calculated as the mean of all points on the segmentation mask in each rope segment (Figure 12c).

The rope manipulation task requires deforming a rope segment to match a desired goal shape specified by eight keypoints evenly spaced on the rope. Leveraging the PyFleX simulator [39], we collected 6×10^4 transition pairs generated through random interaction as the dataset (Figure 13c). We adopt a similar formulation as in the object pushing task, using a three-layer MLP with 256 hidden units in each layer for the dynamics model, trained with the mean squared error loss between the predicted state and the ground truth state at the next time step. For the regularization terms, we follow Equation 12 with $\lambda_{\text{ReLU}} = 2 \times 10^{-3}$, $\lambda_{\text{ID}} = 5 \times 10^{-5}$, and $\lambda_{\text{reg}} = 1 \times 10^{-4}$. We optimize the full model with an Adam optimizer [32] with a learning rate of 5×10^{-4} until convergence, then train each subsequent sparsified model for 500 epochs.